Open Ceramics 15 (2023) 100402

Contents lists available at ScienceDirect

Open Ceramics

journal homepage: www.sciencedirect.com/journal/open-ceramics

# Chemistry, structure, and thermodynamic stabilization of SiOC polymer derived ceramics made from commercial precursors

Gerson J. Leonel [a,b], Xin Guo [a], Gurpreet Singh [c], Alexandra Navrotsky [a,b,*]

[a] School of Molecular Sciences and Center for Materials of the Universe, Arizona State University, Tempe, AZ, 85287, USA
[b] Navrotsky Eyring Center for Materials of the Universe, School of Molecular Sciences, Arizona State University, Tempe, AZ, 85287, USA
[c] Mechanical and Nuclear Engineering Department, Kansas State University, 3002 Rathbone Hall, Manhattan, KS, 66506, USA

ARTICLE INFO

Handling Editor: Dr P Colombo

ABSTRACT

This study explores the energetics and structure of polymer derived ceramics (PDCs) derived from the pyrolysis of preceramic polymers: SPR-212 (SPR), polyhydromethylsiloxane (PHMS) blend, and 1,3,5,7-tetravinyl-1,3,5,7-tetramethylcyclotetrasiloxane (TTCS) at 1200 and 1500 °C. There are close similarities in the composition of PDCs derived from PHMS (blend) and SPR-212 at 1200 °C, but high-resolution X-ray photoelectron spectroscopy shows notable differences in their microstructure. Enthalpies of formation ($\Delta H^{\circ}_{f,elem}$) of SPR-1200, TTCS-1200, PHMS-1200, SPR-1500, TTCS-1500, and PHMS-1500 are -154.40 ± 3.19, -116.35 ± 3.48, -197.55 ± 3.05, -170.12 ± 3.50, -167.29 ± 3.35, and -212.43 ± 2.71 kJ $mol^{-1}$, respectively. PDCs derived from low-cost commercial precursors (PHMS blend) appear to be more thermodynamically stable than those derived from an industrial preceramic polymer (SPR-212). Thermodynamic stability of the SiOCs increases with pyrolysis temperature. The results suggest that differences in silicon mixed bonding environments and their relative amounts ($SiO_3C$, $SiO_2C_2$, or $SiOC_3$) lead to differences in thermodynamic stabilization.

## 1. Introduction

Recently, there has been significant increase in research for ultrahigh temperature materials, especially for application in the aerospace industry [1,2], where stable materials capable of withstanding high temperatures during re-entry are needed [3,4]. SiOC ceramics are suitable candidates due to their robust chemical, structural, and thermal stability [5–7]. One method for the synthesis of such ceramics, relies on the high temperature sintering of silica and graphite ceramic powder mixtures [8–10]. This reaction requires high synthesis temperatures [11–13]. This approach does not provide efficient tunability of the shape, composition, microstructure, and properties. These factors make it less attractive for the industrial scale.

PDCs are derived from the high temperature pyrolysis of preceramic polymers [14–17]. A significant advantage of the PDC route is the ease in tunability of composition, microstructure, and dimensionality of the ceramic material [18–20]. Tunability of microstructure can be achieved simply by varying the pendant groups attached to the backbone of the polymeric precursor [21,22]. Tunability in the dimensions of the precursor permits efficient manufacturing of low dimensional structures such as thin films and ceramic fiber mats. This is possible by use of electrospinning, chemical vapor deposition, 3D printing, and other additive manufacturing techniques [23,24]. Additionally, the PDC route permits efficient design and synthesis of various systems including SiCN and Si(B)CN, which cannot easily be synthesized by conventional ceramic powder processing methods [25–27].

The thermal and chemical stabilities of PDCs are only some of the features contributing to their recent increase in popularity [6,28]. As the application of these materials in different industries gains more significance, it is important to understand how different preceramic polymers affect the composition and microstructure of pyrolyzed ceramic. These differences are likely to result in the formation of different nanoscale domains and interfacial interactions [26,29,30]. These modifications can be associated with changes in the free energy of systems [31]. Currently, it is understood that greater amounts of mixed bonding (Si bonded to both C and O) in the microstructure of precursor derived ceramics, like SiOC, SiCN, and SiOCN is consistent with greater thermodynamic stability [32,33]. However, only few reports have investigated the stabilization promoted by different mixed bonding configurations ($SiO_3C$, $SiO_2C_2$, and $SiOC_3$) [21,33].

Not many studies have investigated whether similar compositions and microstructure of SiOC PDCs derived from industrial precursors can

* Corresponding author. School of Molecular Sciences and Center for Materials of the Universe, Arizona State University, Tempe, AZ, 85287, United States.
*E-mail address:* Alexandra.Navrotsky@asu.edu (A. Navrotsky).

https://doi.org/10.1016/j.oceram.2023.100402
Received 6 December 2022; Received in revised form 30 May 2023; Accepted 30 June 2023
Available online 1 July 2023

be achieved from pyrolysis of low-cost commercial preceramic polymers. In this work we investigate the composition, structure, and thermodynamic stability of SiOCs derived from industrial precursor (SPR-212), as well as two low-cost preceramic polymers: polyhydromethylsiloxane (PHMS) polymer blend and tetramethylcyclotetrasiloxane (TTCS). Polymer derived SiOC ceramic is a general term that describes ceramics that contain free carbon in the $SiO_xC_{4-x}$ mixed bonds (where, $0 \leq x \leq 4$) matrix. It should be noted that some SiOCs can have near stoichiometric compositions while others can have excess silicon [34–37]. This investigation permits assessment of how structure of polymeric precursors translates to compositional and microstructural differences in the SiOC ceramics. SPR-212 is a linear polymer and single source industrial precursor of SiOCs. The as obtained polymer can undergo low temperature curing at ~230 °C without the addition of a catalyst. The low viscosity of the precursor permits its use in applications including molding, coatings, and matrix composites [38–40]. TTCS is a cyclic single source commercial precursor for development of PDCs with potential application as Li-ion battery anodes [41,42]. Different PHMS polymer blends have been explored and are of interest for the synthesis of high temperature ceramics [43–45].

In this study, six SiOC samples are investigated, SPR-1200, TTCS-1200, PHMS-1200, SPR-1500, TTCS-1500, and PHMS-1500. This work reports the synthesis, characterization, and thermodynamic analysis of the PDCs synthesized at 1200 and 1500 °C. All samples are obtained from pyrolysis of polymeric precursors under inert atmosphere. There are systemic differences in the composition and microstructure of the samples, which lead to differences in thermodynamic stability. By systematically exploring these samples, it is possible to identify structural descriptors in preceramic polymers and PDCs contributing to the formation of SiOCs with thermodynamically more stable microstructures. This investigation identifies differences in the stabilization promoted by $SiO_3C$, $SiOC_3$, and $SiO_2C_2$ mixed bonding configurations. Structural characterization of the samples is done by Fourier transform infrared spectroscopy (FTIR), X-ray photoemission spectroscopy (XPS), high resolution XPS (HR-XPS), and Raman spectroscopy. High temperature oxide melt solution calorimetry is employed for assessment of thermodynamic stability of the materials.

## 2. Experimental methods

### 2.1. Materials

Ceramics are derived from polymeric precursors: SPR-2012 (SPR) from Starfire Systems, 1,3,5-trivinyl-1,1,3,5,5-pentamethyltrisiloxane (TPTS), 1,3,5,7-tetravinyl-1,3,5,7-tetramethylcyclotetrasiloxane (TTCS), and polyhydromethylsiloxane (PHMS), from Gelest, Inc. The Si: O ratio in SPR, TPTS, PHMS, and TTCS are 4 : 5, 3 : 2, 3 : 2, and 4 : 4, respectively. dicumyl peroxide (DCP) and platinum(0)-1,3- divinyl-1,1,3,3-tetramethyldisiloxane (DVD) are used as crosslinking catalysts. Structure of the oligomers is shown in Fig. 1.

### 2.2. Crosslinking

A blend of two oligomers: PHMS plus 40 wt% TPTS and 1 wt% DVD, is employed as precursor for PHMS-derived SiOCs. SPR-212 is used as a single source industrial precursor (without the addition of catalyst) for synthesis of the SPR PDCs. TTCS-derived ceramics are obtained from mixture of TTCS plus 1 wt% DCP. All oligomers are crosslinked into infusible solid precursors at ~300 °C, under inert atmosphere.

### 2.3. Pyrolysis

Pyrolysis of the crosslinked precursors uses a Netzsch STA 409 differential scanning calorimeter cell, using alumina crucibles. This allows accurate temperature control with low temperature gradients. The samples are heated from ambient to the final pyrolysis temperature at a ramp rate of 2 °C/min, under flowing argon (~50 mL/min). During temperature ramping, each sample is held at 400 °C for 1 h, this ensures complete crosslinking of the precursor. Thermolysis of precursors is investigated at 1200 and 1500 °C, and resulted in the formation of SPR-1200, TTCS-1200, PHMS-1200, SPR-1500, TTCS-1500, and PHMS-1500 SiOCs. The PDCs are then ground into powders.

### 2.4. Characterization

FTIR experiments are performed by employing a bench-top Bruker TENSOR with platinum ATR accessory. Spectra are collected in the range of 4000-500 $cm^{-1}$. X-ray diffraction (XRD) experiments are conducted at ambient temperature using a bench-top Bruker D2 powder diffractometer employing a nickel-filtered CuKα radiation (wavelength = 1.5418 Å). Elemental analysis of the ceramic powders employs X-ray photoelectron spectroscopy (XPS). XPS experiments are performed by use of a Kratos AXIS Supra+ with a monochromatic Al Kα+ ion beam (beam energy = 1486.6 eV). Raman spectroscopy uses a custom-built multi-wavelengths system with a 532 nm green laser at a power of 74 mW with a 50 X microscope objective. TG-DSC experiments employ a Setaram LABSYS Evo DTA/DSC.

### 2.5. Thermochemistry

In this study, the thermodynamic stability of the PDCs is assessed by thermochemical calculations of enthalpies of formation from elements ($\Delta H^\circ_{f,\ elem}$) and crystalline components ($\Delta H^\circ_{f,\ comp}$). Enthalpies of dissolution ($\Delta H_{dis}$) are obtained from calorimetric experiments by employing a commercial twin Calvet type Seteram Alexsys calorimeter. Due to the high solubility of the PDCs in the oxide melt, 20 g of sodium

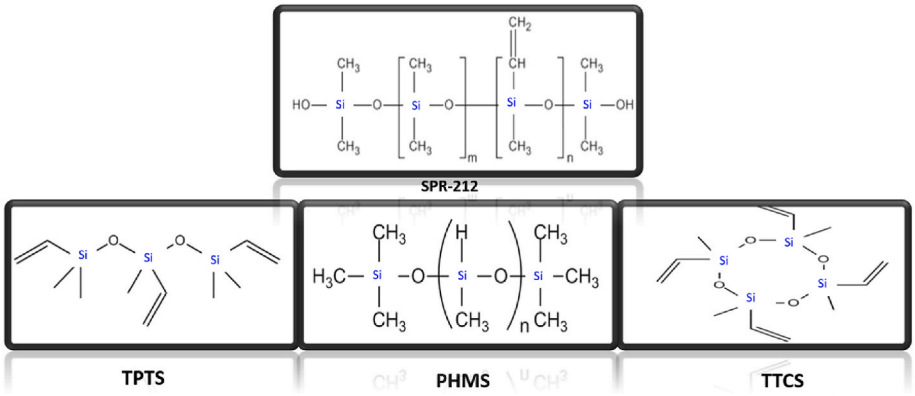


**Fig. 1.** Structure of oligomers used for synthesis of the ceramic powders at 1200 and 1500 °C, under argon atmosphere.

**Table 1**
Thermochemical cycle for calculation of enthalpy of formation from elements $\Delta H^{\circ}_{f,\ elem.}$

| Enthalpies of formation from the elements ($\Delta H_{f,\ elem}$)<br>a Si(s, 25 °C) + b/2 $O_2$(g, 25 °C) + c C (s, 25 °C)→ $Si_aO_bC_c$ (s, 25°C) $\Delta H^{\circ}_{f,\ elem}$ = ? | ΔH (kJ/mol) |
|---|---|
| $Si_a$ $O_b$ $C_c$ (s, 25 °C) + (((2a) + (2c)-b))/2) $O_2$ (g, 800 °C) → a $SiO_2$ (s, 800 °C) + c $CO_2$ (g, 800 °C) | $\mathbf{\Delta H_{dis,\ SiOC}}$ |
| Si (s, 25 °C) + $O_2$ (g, 800 °C) → $SiO_2$ (s, 800 °C) | $\Delta H_2$ = -883.13 ± 2.1 |
| C (s, 25 °C) + $O_2$ (g, 800 °C) → $CO_2$ (g, 800 °C) | $\Delta H_3$ = -381.35 ± 0.13 |
| $O_2$ (g, 25 °C) → $O_2$ (g, 800 °C) | $\Delta H_4$ = 25.34 ± 0.10 |
| $\mathbf{\Delta H^{\circ}_{f,\ elem} = -\Delta H_{dis,\ SiOC} + a\ \Delta H_2 + c\ \Delta H_3 + (b/2)\ \Delta H_4}$ | $\mathbf{\Delta H^{\circ}_{f,\ elem}}$ |

molybdate ($3Na_2O{\cdot}MoO_3$) melt, at 800 °C are employed for oxidative dissolution. For each experiment, about 5 mg of sample are weighed using a Mettler Toledo microbalance with 10 μg accuracy. The weighed samples are pressed into a pellet using a 1.5 mm tungsten die. The pellets are then inserted into the melt for oxidative dissolution. The melt is continuously bubbled with 40 mL/min of oxygen, to maintain an oxidative environment. The gases evolved from dissolution of the sample are evacuated from the calorimeter by utilizing oxygen flushing at a flowrate of 100 mL/min. To ensure reproducibility, the experiments are repeated at least four times. This is a well-established technique that has been previously used to investigate similar systems [46–49].

Reaction (1) describes the oxidative dissolution of SiOCs.

$$Si_a\ O_b\ C_c\ (s, 25\ ^{\circ}C) + (((2a) + ((2c)-b)/2)\ O_2\ (g, 800\ ^{O}C) \rightarrow a\ SiO_2\ (s, 800\ ^{\circ}C) + c\ CO_2\ (g, 800\ ^{\circ}C)\ \Delta H_{dis,\ SiOC} \quad (1)$$

Enthalpy of formation of the SiOCs from the elements (Si, C, and $O_2$) is described by:

$$a\ Si(s, 25\ ^{\circ}C) + b/2\ O_2(g, 25\ ^{\circ}C) + c\ C\ (s, 25\ ^{\circ}C) \rightarrow Si_aO_bC_c\ (s, 25^{\circ}C)\ \Delta H^{\circ}_{f,\ elem} \quad (2)$$

Enthalpy of formation relative to crystalline components (β-SiC, $SiO_2$ (cristobalite), and C (graphite)) is described by:

$$(a-(b/2))\ SiC(s, 25\ ^{\circ}C) + (b/2)\ SiO_2(s, 25\ ^{\circ}C) + (c-(a-(b/2)))\ C\ (s, 25\ ^{\circ}C) \rightarrow Si_aO_bC_c\ (s, 25^{\circ}C)\ \Delta H^{\circ}_{f,\ comp} \quad (3)$$

During dissolution, Si is oxidized and precipitates as cristobalite and C is oxidized into $CO_2$. Both $CO_2$ and $O_2$ evolve from the melt as gases [33,50,51]. The gaseous oxides have very low solubility in the melt [33,50,51]. By identifying the initial and final state of the system, enthalpies of dissolution ($\Delta H_{dis,\ SiOC}$) and thermodynamic cycles (see Tables 1-2) are employed to calculate enthalpies of formation.

## 3. Results and discussion

FTIR permits identification of functional groups in the structure of pre-ceramic polymers and corresponding PDCs [52–54]. The high energy of the beam identifies vibrations corresponding to strong bonds with low polarizability like C–O and O–H, which are otherwise hard to observe by Raman spectroscopy. The spectra of crosslinked precursors (see Fig. 2A) suggest presence of Si–O–Si (~1060 $cm^{-1}$) and Si–$CH_3$ (~1260 $cm^{-1}$) bond stretching, as well as other functional groups consistent with structure of the preceramic polymers [52–54]. The results point to evolution of organic groups during high temperature treatment of the polymeric precursors, as peaks corresponding to C–H and Si–H bonds are not detected in the spectra of samples pyrolyzed at 1200 and 1500 °C (see Fig. 2B). Spectra of the ceramic powders (Fig. 2B) suggest the presence of C═C (~1600 $cm^{-1}$), Si–O–Si (~1060 $cm^{-1}$), and Si–C (~800 $cm^{-1}$) bond stretch vibrational bands. These results are consistent with the structure of SiOCs [55–60].

Thermal analysis of the precursors is conducted by use of TG-DSC (50 mL/min flowing argon atmosphere, 10 °C/min temperature ramping). The analyses are only conducted up to 1000 °C due to equipment limitations. The results in Fig. 3 point to significant mass loss in all specimens up to ~800 °C, which results from evolution of volatile organics. SPR-212 and PHMS (blend) display comparable TG-DSC curves, with major mass loss occurring near ~ 500 °C. In contrast TTCS displays greatest mass loss at a lower temperature (~ 425 °C). The exothermic DSC peaks near ~300 °C likely correspond to crosslinking [61]. Other exothermic peaks beyond 400 °C may result from the ceramization step [62]. The results suggest that the trend in ceramization temperature is: PHMS (~550 °C) > SPR (~450 °C) > TTCS (~425 °C). This highlights the lower ceramization temperature in TTC precursors. The specimens do not display significant mass loss beyond ~800 °C, which is typical in PDCs [63]. The larger mass loss of TTCS may in part result from the release of greater amounts of hydrogen and/or water during ceramization. We cannot determine other specific reasons for the greater mass loss in TTCS.

We employ XRD for detecting the presence or absence of crystalline (or poorly crystalline) phases in samples synthesized at high temperatures. The patterns (see Fig. 4) confirm the formation of amorphous structures in samples synthesized at 1200 °C. The broad peaks in the spectra of PDCs synthesized at 1500 °C suggest nucleation and growth of poorly crystalline β-SiC grains upon increase in pyrolysis temperature [30]. The exposure of SiOC PDCs to high temperatures (>1400 °C) typically results in carbothermal reduction, which occurs in parallel to growth of crystalline domains [64–66]. These results are in line with previous studies investigating similar materials [33,67,68].

Raman spectra (Fig. 5) identify the types of carbon present in the microstructure of PDCs. D (~1330 $cm^{-1}$) and G (~1600 $cm^{-1}$) bands correspond to $sp^2$-hybridized disordered and graphitic-like carbons, respectively [23,30]. The integrated intensity of the full width at half maximum (FWHM) of the D($I_D$) and G ($I_G$) bands permits identification of the ratio of disordered carbon D($I_D$) to graphitic carbon G ($I_G$) [30,31]. There is significant increase in the relative amount of graphitic (well-ordered) carbon with synthesis temperature (see Table 3). Curve fitting of the spectra permits identification of T (1204–1232 $cm^{-1}$) and D" (1490–1504 $cm^{-1}$) bands, which correspond to considerable amounts of $sp^2$-$sp^3$ bonds and amorphous carbon, respectively [23]. Fig. 5 suggest significant decrease in the relative amount of $sp^2$-$sp^3$ bonds and amorphous carbons in the microstructure of samples synthesized at

**Table 2**
Thermochemical cycle for calculation of enthalpy of formation from components $\Delta H^{\circ}_{f,\ comp.}$

| Enthalpies of formation from components ($\Delta H_{f,\ comp}$)<br>(a-(b/2)) SiC(s, 25 °C) + (b/2) $SiO_2$(s, 25 °C) + (c-(a-(b/2))) C (s, 25 °C)→ $Si_aO_bC_c$ (s, 25°C) $\Delta H^{\circ}_{f,\ comp}$ = ? | ΔH (kJ/mol) |
|---|---|
| $Si_a$ $O_b$ $C_c$ (s, 25 °C) + (((2a) + ((2c)-b)/2) $O_2$ (g, 800 °C) → a $SiO_2$ (s, 800 °C) + c $CO_2$ (g, 800 °C) | $\mathbf{\Delta H_{dis,\ SiOC}}$ |
| $SiO_2$ (S, 25 °C) → $SiO_2$ (s, 800 °C) | $\Delta H_2$ = 50.1 ± 0.10 |
| SiC (S, 25 °C) + $2O_2$ (g, 800 °C) → $SiO_2$ (s, 800 °C) + $CO_2$ (g, 800 °C) | $\Delta H_3$ = -1192.28 ± 2.15 |
| C (S, 25 °C) + $O_2$ (g, 800 °C) → $CO_2$ (g, 800 °C) | $\Delta H_4$ = -381.35 ± 0.13 |
| $\mathbf{\Delta H^{\circ}_{f,\ comp} = -\Delta H_{dis,\ SiOC} + (b/2)\ \Delta H_2 + (a-(b/2))\ \Delta H_3 + (c-(a-(b/2)))\ \Delta H_4}$ | $\mathbf{\Delta H^{\circ}_{f,\ comp}}$ |

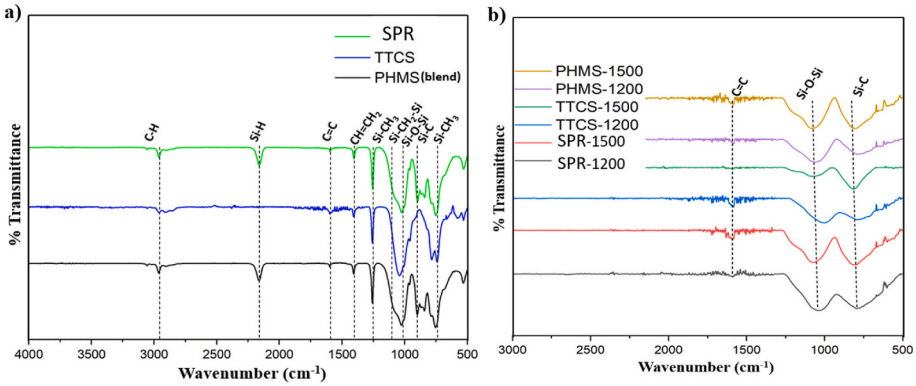


**Fig. 2.** FTIR spectra of a) crosslinked polymeric precursors and b) SiOCs synthesized at 1200 and 1500 °C.

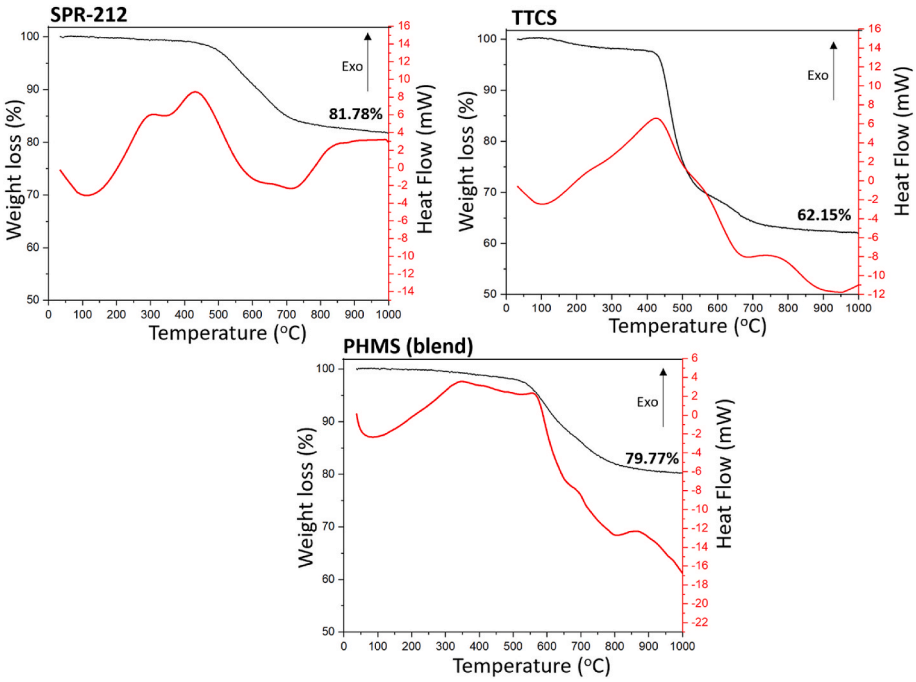


**Fig. 3.** TG-DSC curves of crosslinked precursors.

1500 °C. Disorder induced D' bands (~1620 $cm^{-1}$) are only observed in the spectrum of SPR-1200 [69].

XPS permits elemental analysis as well as identification of bonding speciation in the structure of fine powders [30]. Identification of speciation and semi-quantitative assessment of their relative amounts is achieved by probing Si 2*p*, O 1*s*, and C 1*s* bonds [70]. Coupled with other characterization techniques such as Raman, XPS allows identification of differences in the microstructure of the PDCs synthesized at varying temperatures [30]. By employing appropriate curve fitting, the area under each convolution represents the relative amount of the types of bonds. HR-XPS spectra of the samples are shown in Fig. 6.

C 1*s* convolutions show that all samples contain considerable amounts of C–O (~286.5 eV) and C–C (~285 eV) and C–Si (283.7 eV) bonds [71,72]. In mixed bonding C is bonded to Si or to another C, and typically free carbon does not bond with significant amounts of oxygen. Therefore the C–O bonds may correspond to bond signatures from foreign carbon-containing impurities such as lint, pollen, or strongly bound $CO_2$, as previously reported [73–75]. This makes semi-quantitative analysis of C 1s bonds by XPS alone challenging [72,73]. It is likely that C–Si convolutions also include bonds formed in SiC domains. Similarly, the presence of C–C bonds is consistent with Raman spectra (see Fig. 5) and may correspond to free carbon or to C–C terminated mixed bonding. Si *2p* convolutions of samples pyrolyzed at 1200 °C suggest the presence of significant amounts of $SiO_4$ (~104 eV), $SiO_2C_2$ (~102 eV), and $SiO_3C$ (~102.9 eV), and $SiOC_3$ (~ 101 eV) bonds [71,76]. $SiO_4$ correspond to amorphous $SiO_2$ (silica) domains and $SiO_xC_{4-x}$ correspond to mixed bonding networks (Si bonded to both C and O) [77]. From the samples synthesized at 1200 °C, SPR-1200 appears to have the greatest relative amount of $SiO_4$ bonds, while PHMS-1200 and TCCS-1200 display greatest relative amount of $SiO_xC_{4-x}$ mixed bonding environments. The spectra further show that for samples synthesized at 1500 °C, the relative amount of $SiO_4$ (silica) bonds is greatest in PHMS-1500, although SPR-1500, and TTCS-1500 also display large relative amount of $SiO_4$ bonds compared to their analogues synthesized at lower temperature. This may indicate significant phase separation in the amorphous structures to form stoichiometric domains ($SiO_2$ and SiC) with increase in synthesis temperature. Additionally, the results in Fig. 6 point to a decrease in the amount of $SiO_3C$ relative to $SiO_2C_2$ and/or $SiOC_3$ mixed bonds, between 1200 and 1500 °C. This may suggest lower stability of $SiO_3C$ compared to other mixed bonding networks.

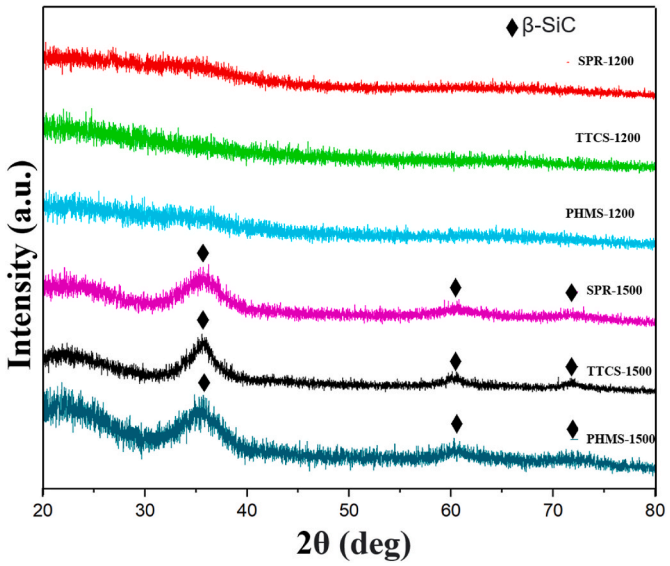


**Fig. 4.** XRD patterns show growth of beta-SiC crystals in PDCs synthesized at 1500 °C. The spectra do not show peaks corresponding to graphite. This suggests that any free carbon may be present as amorphous domains.

### 3.1. Elemental analysis

Thermodynamic analysis of PDCs requires accurate elemental compositions. XPS survey scans are useful in obtaining compositional information of fine ceramic powders synthesized at high temperatures, when residual hydrogen (if any) is scarce. The results from elemental analysis are summarized in Table 4. It is apparent that the Si: O ratio increases with pyrolysis temperature. In contrast, the Si: C ratio decreases with temperature. These results likely correspond to carbothermal reduction in the samples pyrolyzed at higher temperature (1500 °C). During carbothermal reduction $SiO_2$ domains react with excess free carbon phase to produce $CO_2$ (gas) and SiC. These results are consistent with the XRD pattern (see Fig. 4) of samples pyrolyzed at 1500 °C, which point to growth of β-SiC grains. XPS compositions are employed for thermodynamic analysis discussed in the section that follows.

**Table 3**
Summary of D/G in the PDCs.

| sample | D ($I_D$)/G ($I_G$) (FWHM) |
|---|---|
| SPR-1200 | 1.57 |
| TTCS-1200 | 1.94 |
| PHMS-1200 | 1.77 |
| SPR-1500 | 1.00 |
| TTCS-1500 | 1.33 |
| PHMS-1500 | 1.11 |

The results from elemental analysis suggest that pyrolysis of the PHMS (blend) at 1200 °C results in formation of SiOC with a composition and phase assemblage closest to that of the sample derived from SPR-212 industrial precursor (see Table 5). In contrast, there is significant difference of bonding speciation in their microstructure (from HR-XPS Si *2p* convolutions). No obvious similarities in composition and phase assemblage are observed in the samples synthesized at 1500 °C. Calorimetric experiments permit systematic assessment of the effect of

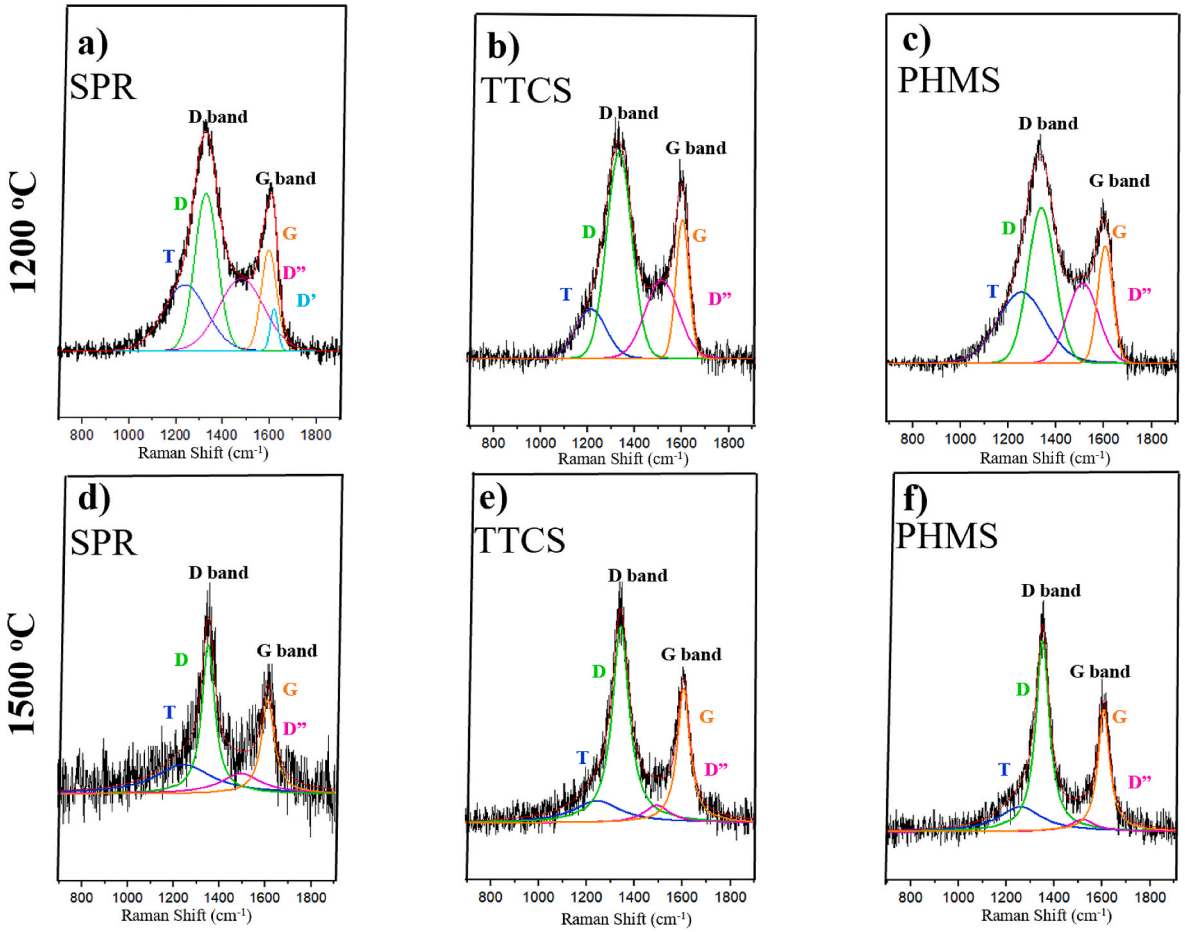


**Fig. 5.** Raman spectra of a) SPR-1200, b) TTCS-1200, c) PHMS-1200, d) SPR-1500, e) TTCS-1500, f) PHMS-1500.

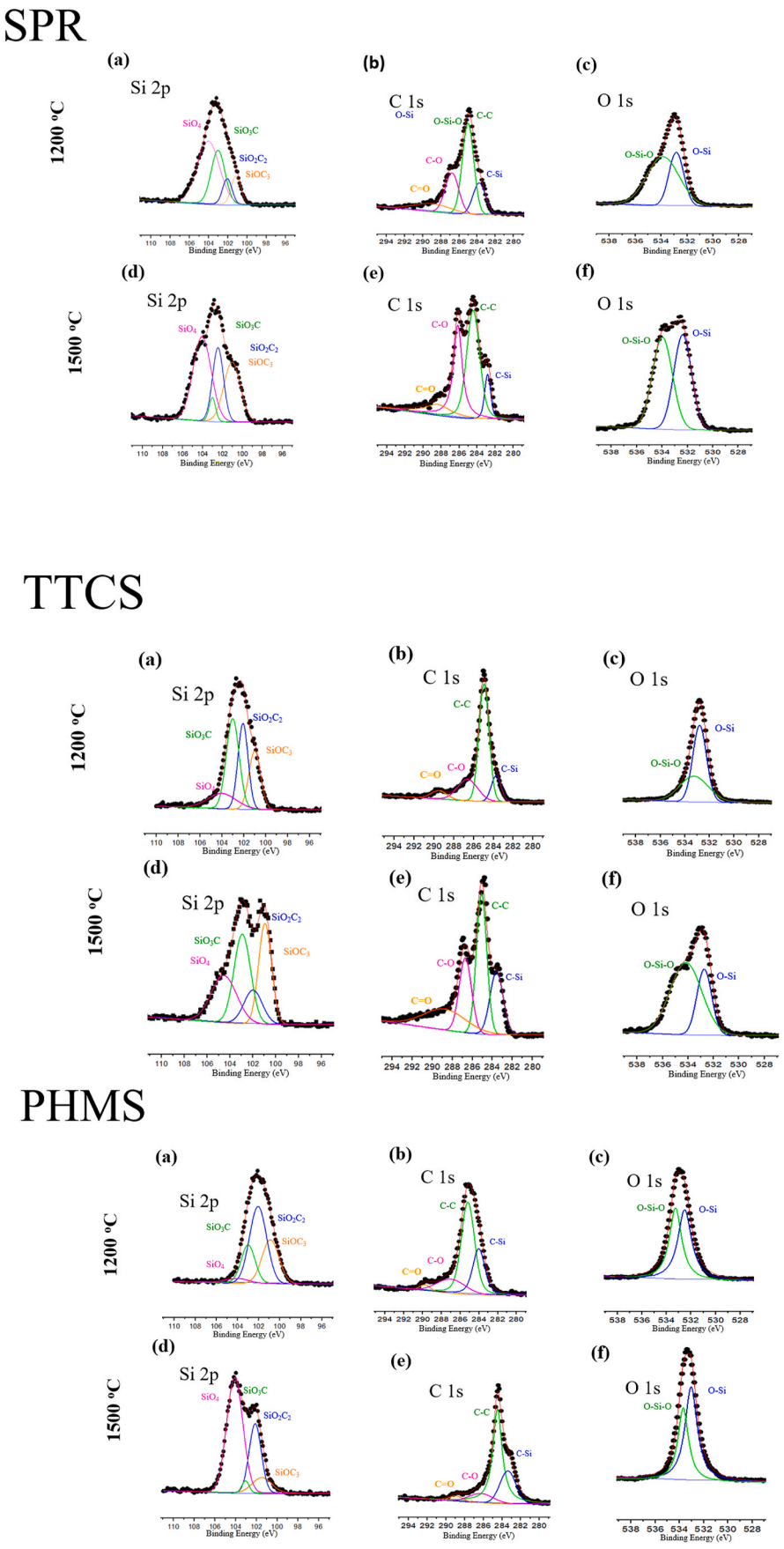


**Fig. 6.** HR XPS of SPR, TTCS and PHMS derived ceramics.

**Table 4**
Elemental analysis of SiOC samples from XPS survey scans.

| Elemental Composition by XPS | | | |
|---|---|---|---|
| | Elements (at.%) | | |
| SiOC sample | C 1s | O 1s | Si 2p |
| SPR-1200 | 35.47 ± 1.11 | 30.56 ± 1.21 | 33.97 ± 0.1 |
| SPR-1500 | 37.12 ± 0.04 | 27.32 ± 1.48 | 35.56 ± 1.46 |
| TTCS-1200 | 50.28 ± 0.44 | 25.29 ± 1.24 | 24.43 ± 0.49 |
| TTCS-1500 | 48.76 ± 1.04 | 19.37 ± 0.1 | 31.87 ± 0.94 |
| PHMS-1200 | 38.16 ± 0.61 | 30.25 ± 2 | 31.62 ± 1.07 |
| PHMS-1500 | 40.35 ± 2.55 | 28.57 ± 2.96 | 31.15 ± 0.11 |

**Table 5**
Composition and estimated phase assemblage of SiOCs derived from SPR-212, TTCS, and PHMS at 1200 and 1500 °C.

| Sample | Composition $Si_xO_yC_z$ (x + y + z = 1) | $SiO_2$ (mol%) | SiC (mol%) | C (mol%) |
|---|---|---|---|---|
| SPR-1200 | $Si_{0.34}O_{0.31}C_{0.35}$ | 30.69 | 36.63 | 32.67 |
| TTCS-1200 | $Si_{0.25}O_{0.25}C_{0.50}$ | 20 | 20 | 60 |
| PHMS-1200 | $Si_{0.32}O_{0.30}C_{0.38}$ | 28.30 | 32.07 | 39.62 |
| SPR-1500 | $Si_{0.36}O_{0.27}C_{0.37}$ | 26.73 | 44.55 | 28.71 |
| TTCS-1500 | $Si_{0.32}O_{0.19}C_{0.49}$ | 16.24 | 38.46 | 45.30 |
| PHMS-1500 | $Si_{0.31}O_{0.29}C_{0.40}$ | 26.60 | 30.27 | 43.12 |

composition and microstructure (including phase assemblage) on the thermodynamic stability of SiOCs. These results indicate that PDCs derived from the PHMS blend display the smallest change in composition, between 1200 and 1500 °C, even compared to samples derived from industrial precursor (SPR-212). This could point to higher stability of the PHMS-1200.

### 3.2. Energetics of formation and interdomain interactions

The results from thermodynamic analysis of the SiOCs are summarized in Table 6. Overall, enthalpies of dissolution become more negative with increasing C and Si content, which results from highly exothermic oxidation of these elements. Enthalpies of formation permit identification of trends in the thermodynamic stability of the samples. More exothermic enthalpies of formation correspond to greater thermodynamic stability, as entropic effects are relatively small in comparison to the highly exothermic enthalpies of formation from the elements [30,31]. For samples synthesized at 1200 and 1500 °C, enthalpies of formation from elements ($\Delta H^{\circ}_{f,\ elem}$) are most exothermic for samples derived from the PHMS (blend) precursor and least for PDCs derived from TTCS. This points to greatest enthalpic drive for the formation of the microstructure in PHMS-1500.The results further suggest that pyrolysis of the industrial SiOC precursor (SPR-212), results in formation of microstructures (SPR-1200 and SPR-1500) with intermediate stability relative to elements.

Table 6 also presents enthalpies of formation relative to components ($\Delta H^{\circ}_{f,\ comp}$), namely β-SiC, $SiO_2$ (cristobalite), and C (graphite). More exothermic enthalpy of formation from components corresponds to energetically more favorable interdomain interaction and/or greater amount of mixed bonding (supported by XPS convolutions) [30,31]. Mixed bonding promotes greater stabilization of microstructures as a result of less bond strain compared to the interface between stoichiometric crystalline domains. The results show that for samples synthesized at 1200 °C, $\Delta H^{\circ}_{f,\ comp}$ is most exothermic for PHMS-1200 and least for TTCS-1200. Similarly, the results point to little energetically favorable interdomain interactions in SPR-1200. However, increasing synthesis temperature to 1500 °C, results in structural evolution suggesting highly favorable interdomain interaction and/or mixed bonding in the microstructure of SPR-1500, TTCS-1500, and PHMS-1500. At all temperatures PDCs derived from low-cost preceramic polymers PHMS (blend) result in structures with highest thermodynamic stability, even compared to samples derived from industrial precursor (SPR-212). Note that the positive enthalpy for the formation of TTCS-1200 could indicate unfavorable interdomain interactions, however, it appears that the interactions become less unfavorable at 1500 °C, hence the more exothermic formation enthalpy in TTCS-1500. This complexity, perhaps related to both changes in domain structure and coarsening, may explain the superior stabilization of TTCS-derived SiOC in this temperature range. Structural characterization suggests that compositional changes are driven by carbothermal reduction. Compared to the other samples synthesized at 1200 °C, the higher C content and O/Si ratio in TTCS-1200 may provide greater drive for that reaction.

### 3.3. Link between microstructure and thermodynamic stability of PDCs

FTIR, XRD, Raman, and XPS all show that SiOCs derived from all three polymeric precursors undergo significant structural modifications between 1200 and 1500 °C Similarly, thermodynamic analysis (Table 6), shows increase in thermodynamic stability of the SiOCs with increasing pyrolysis temperature, independent of initial precursor. This shows that between 1200 and 1500 °C, the PDCs evolve towards thermodynamically more stable structures. For all synthesis temperatures, greater O content is consistent with greater thermodynamic stability (see $\Delta H^{\circ}_{f,\ elem}$). This may result from greater amounts of $SiO_2$ and/or $SiO_xC_{4-x}$ mixed bonding domains (supported by HR-XPS convolutions). This highlights correlation between bonding speciation and thermodynamic stabilization.

It is important to stress the decrease in the O content of PDCs synthesized at 1500 °C (from elemental analysis), which occur in parallel with growth and nucleation of β-SiC grains (from XRD). The thermodynamic analysis suggests that growth/crystalization of β-SiC domains is thermodynamically favorable and occurs in parallel with increase in favorable interdomain interactions. This points to significant thermodynamic drive for carbothermal reduction in SiOCs to form more SiC.

Similarly, results from Raman spectroscopy (see Fig. 5) indicate significant decrease in the relative amount of $sp^2$-$sp^3$ carbon bonds (T bands) as well as disordered carbons (from the ratio of D ($I_D$)/G ($I_G$) at FWHM) in samples synthesized at 1500 °C. This may point to consumption of amorphous free carbons during carbothermal reduction and/or formation of well-defined carbon networks at higher pyrolysis temperature. Additionally, HR-XPS convolutions and the phase assemblages suggest presence of significant amount of C–C bonds in all samples. This may imply that decrease in intensity of D" bands for high

**Table 6**
Summary of enthalpies of dissolution ($\mathbf{\Delta H_{dis}}$), enthalpies of formation from elements ($\mathbf{\Delta H^{\circ}_{f,\ elem}}$), and enthalpies of formation from components ($\mathbf{\Delta H^{\circ}_{f,\ comp}}$).

| Sample | Composition $Si_xO_yC_z$(x + y + z = 1) | $\Delta H_{dis}$(kJ.mol$^{-1}$) | $\Delta H^{\circ}_{f,\ elem}$ (kJ.mol$^{-1}$) | $\Delta H^{\circ}_{f,\ comp}$ (kJ.mol$^{-1}$) |
|---|---|---|---|---|
| SPR-1200 | $Si_{0.34}O_{0.31}C_{0.35}$ | −275.41 ± 2.40 | −154.40 ± 3.19 | −0.31 ± 3.23 |
| TTCS-1200 | $Si_{0.25}O_{0.25}C_{0.50}$ | −291.94 ± 2.77 | −116.35 ± 3.48 | +6.16 ± 3.51 |
| PHMS-1200 | $Si_{0.32}O_{0.30}C_{0.38}$ | −226.92 ± 2.21 | −197.55 ± 3.05 | −48.34 ± 3.09 |
| SPR-1500 | $Si_{0.36}O_{0.27}C_{0.37}$ | −284.91 ± 2.78 | −170.12 ± 3.50 | −31.88 ± 3.52 |
| TTCS-1500 | $Si_{0.32}O_{0.19}C_{0.49}$ | −299.76 ± 2.60 | −167.29 ± 3.35 | −64.80 ± 3.38 |
| PHMS-1500 | $Si_{0.31}O_{0.29}C_{0.40}$ | −210.21 ± 1.70 | −212.43 ± 2.71 | −68.87 ± 2.74 |

temperature (1500 °C) samples mainly result from formation of well-defined carbon networks. These observations could indicate significant stabilization of structures with decreasing amount of $sp^2$-$sp^3$ carbon bonds and with increase in ordering of the carbon network. HR-XPS convolutions (see Fig. 6) permit identification of variation in bonding speciation with pyrolysis temperature. The results suggest an increase in the amount of $SiO_2C_2$ and/or $SiOC_3$ (relative to $SiO_3C$) mixed bonding with temperature. The increase in thermodynamic stability of the samples with pyrolysis temperature may point to higher stabilizing effect of $SiO_2C_2$ and/or $SiOC_3$ compared to $SiO_3C$ mixed bonding environments. This is important as it permits the identification of an additional descriptor for increased thermodynamics stabilization in PDCs.

### 3.4. Link between structure of preceramic polymers and composition of PDCs

The compositions reported in Table 6 show that SiOCs derived from TTCS (cyclic structure) have the highest carbon content, in contrast, samples derived from SPR-212 (linear structure) display the lowest. TTCS and PHMS (linear polymer blend) precursors have large amounts of less hydrogenated (vinyl compared to methyl) carbonaceous pendant groups (see Fig. 1). Such groups (vinyl, allyl) are expected to form more carbon rich SiOCs upon high temperature pyrolysis, as less carbon is expected to evolve as organics during thermal treatment [78]. Hence, the large amount of methyl instead of vinyl side-groups in the backbone of SPR-212 oligomers may explain the lower C content of SPR-1200 and SPR-1500 samples. Similarly, O content appears to be greatest in SiOCs derived from PHMS blend and SPR-212, and lowest in samples derived from TTCS. The results are consistent with significant loss of low molecular weight carbonaceous side groups ($CH_3$) in the PHMS blend and SPR-212, which ultimately results in increase in O concentration in the PDCs. We do not identify any obvious trends between thermodynamic stability ($\Delta H^\circ_{f,\ comp}$) and overall composition (Si, O, and C content) of the precursors. This is not surprising, as the amounts of different phases and strength of interdomain interactions, which determine the thermodynamic stabilization, are more strongly related to processing history than to bulk composition.

## 4. Conclusion

We report the structure and energetics of SiOCs derived from different preceramic polymers. PDCs derived from PHMS blend have a composition closest to SiOCs synthesized from SPR-212 industrial precursor. The results suggest greatest thermodynamic stability and more favorable interdomain interactions in the microstructure of samples derived from the PHMS blend. For each precursor the increase in energetic stability of specimens synthesized at 1500 °C is also consistent with a decrease in the relative amount of $SiO_3C$ compared to $SiO_2C_2$ and/or $SiOC_3$ mixed bonds. The results highlight increased stabilization of SiOCs with formation of a well-ordered carbon network and decrease in relative amount of $sp^2$-$sp^3$ carbon bonds. This information could serve as a framework for the design of thermodynamically more stable SiOCs.

## Acknowledgments

Financial support from National Science Foundation (NSF) Partnerships for International Research and Education (PIRE) grant #1743701 is gratefully acknowledged. The industrial polymeric precursor (SPR-212) was provided by PIRE partner, Dr. Zlatomir Apostolov.

## References

[1] T.E. Steyer, Shaping the future of ceramics for aerospace applications, Int. J. Appl. Ceram. Technol. 10 (2013) 389–394.
[2] F. Monteverde, A. Bellosi, L. Scatteia, Processing and properties of ultra-high temperature ceramics for space applications, Mater. Sci. Eng. A. 485 (2008) 415–421.
[3] R. Savino, S. Mungiguerra, G.D. Di Martino, Testing ultra-high-temperature ceramics for thermal protection and rocket applications, Adv. Appl. Ceram. 117 (2018) s9–s18.
[4] G. Saccone, R. Gardi, D. Alfano, A. Ferrigno, A. Del Vecchio, Laboratory, on-ground and in-flight investigation of ultra high temperature ceramic composite materials, Aero. Sci. Technol. 58 (2016) 490–497.
[5] Y. Jia, T.D. Ajayi, J. Morales, M.A.R. Chowdhury, G. Sauti, S.-H. Chu, C. Park, C. Xu, Thermal properties of polymer-derived ceramic reinforced with boron nitride nanotubes, J. Am. Ceram. Soc. 102 (2019) 7584–7593.
[6] Z. Ren, S.B. Mujib, G. Singh, High-temperature properties and applications of Si-based polymer-derived ceramics: a Review, Materials 14 (2021) 614.
[7] Z. Zhao, H. Xiang, F.-Z. Dai, Z. Peng, Y. Zhou, P.2O.7 (TiZrHf), An equimolar multicomponent or high entropy ceramic with good thermal stability and low thermal conductivity, J. Mater. Sci. Technol. 35 (2019) 2227–2231.
[8] G.C. Wei, Beta Sic powders produced by carbothermic reduction of silica in a high-temperature rotary furnace, J. Am. Ceram. Soc. 66 (1983) c111–c113.
[9] B.M. Moshtaghioun, R. Poyato, F.L. Cumbrera, S. de Bernardi-Martin, A. Monshi, M.H. Abbasi, F. Karimzadeh, A. Dominguez-Rodriguez, Rapid carbothermic synthesis of silicon carbide nano powders by using microwave heating, J. Eur. Ceram. Soc. 32 (2012) 1787–1794.
[10] L. Carassiti, A. Jones, P. Harrison, P.S. Dobson, S. Kingman, I. MacLaren, D. H. Gregory, Ultra-rapid, sustainable and selective synthesis of silicon carbide powders and nanomaterials via microwave heating, Energy Environ. Sci. 4 (2011) 1503–1510.
[11] A. Taylor, D.S. Laidler, The formation and crystal structure of silicon carbide, Br. J. Appl. Phys. 1 (1950) 174.
[12] R. Ren, Z. Yang, L.L. Shaw, Synthesis of nanostructured silicon carbide through an integrated mechanical and thermal activation process, J. Am. Ceram. Soc. 85 (2002) 819–827.
[13] B.M. Moshtaghioun, A. Monshi, M.H. Abbasi, F. Karimzadeh, A study on the effects of silica particle size and milling time on synthesis of silicon carbide nanoparticles by carbothermic reduction, Int. J. Refract. Met. Hard Mater. 29 (2011) 645–650.
[14] P. Colombo, G. Mera, R. Riedel, G.D. Sorarù, Polymer-derived ceramics: 40 years of research and innovation in advanced ceramics, J. Am. Ceram. Soc. 93 (2010) 1805–1837.
[15] P. Greil, Active-filler-controlled pyrolysis of preceramic polymers, J. Am. Ceram. Soc. 78 (1995) 835–848.
[16] Y.D. Blum, K.B. Schwartz, R.M. Laine, Preceramic polymer pyrolysis, J. Mater. Sci. 24 (1989) 1707–1718.
[17] G.T. Burns, G. Chandra, Pyrolysis of preceramic polymers in ammonia: preparation of silicon nitride powders, J. Am. Ceram. Soc. 72 (1989) 333–337.
[18] L. Hagelüken, P.V.W. Sasikumar, H.-Y. Lee, D. Di Stadio, Y. Chandorkar, M. Rottmar, K. Maniura-Weber, G. Blugan, J. Brugger, Multiscale 2D/3D microshaping and property tuning of polymer-derived SiCN ceramics, J. Eur. Ceram. Soc. 42 (2022) 1963–1970.
[19] W. Duan, X. Yin, Q. Li, L. Schlier, P. Greil, N. Travitzky, A review of absorption properties in silicon-based polymer derived ceramics, J. Eur. Ceram. Soc. 36 (2016) 3681–3689.
[20] E. Ionescu, H.-J. Kleebe, R. Riedel, Silicon-containing polymer-derived ceramic nanocomposites (PDC-NCs): preparative approaches and properties, Chem. Soc. Rev. 41 (2012) 5032–5052.
[21] G. Mera, A. Navrotsky, S. Sen, H.-J. Kleebe, R. Riedel, Polymer-derived SiCN and SiOC ceramics – structure and energetics at the nanoscale, J. Mater. Chem. A. 1 (2013) 3826–3836.
[22] R.P. Chaudhary, C. Parameswaran, M. Idrees, A.S. Rasaki, C. Liu, Z. Chen, P. Colombo, Additive manufacturing of polymer-derived ceramics: materials, technologies, properties and potential applications, Prog. Mater. Sci. 128 (2022), 100969.
[23] Z. Ren, C. Gervais, G. Singh, Fabrication and characterization of silicon oxycarbide fibre-mats via electrospinning for high temperature applications, RSC Adv. 10 (2020) 38446–38455.
[24] S.B. Mujib, R. Cuccato, S. Mukherjee, G. Franchin, P. Colombo, G. Singh, Electrospun SiOC ceramic fiber mats as freestanding electrodes for electrochemical energy storage applications, Ceram. Int. 46 (2020) 3565–3573.
[25] A. Karakuscu, R. Guider, L. Pavesi, G.D. Sorarù, Broad-band tunable visible emission of sol–gel derived SiBOC ceramic thin films, Thin Solid Films 519 (2011) 3822–3826.
[26] G. Mera, A. Tamayo, H. Nguyen, S. Sen, R. Riedel, Nanodomain structure of carbon-rich silicon carbonitride polymer-derived ceramics, J. Am. Ceram. Soc. 93 (2010) 1169–1175.
[27] Y. Yu, Y. Chen, C. Xu, J. Fang, L. An, Synthesis of spherical non-oxide silicon carbonitride ceramic particles, J. Am. Ceram. Soc. 94 (2011) 2779–2782.
[28] R. Bhandavat, Z. Pei, G. Singh, Polymer-derived ceramics as anode material for rechargeable Li-ion batteries: a review, Nanomater. Energy 1 (2012) 324–337.
[29] A.H. Tavakoli, M.M. Armentrout, M. Narisawa, S. Sen, A. Navrotsky, White Si–O–C ceramic: structure and thermodynamic stability, J. Am. Ceram. Soc. 98 (2015) 242–246.
[30] G.J. Leonel, S.B. Mujib, G. Singh, A. Navrotsky, Thermodynamic stabilization of crystalline silicon carbide polymer-derived ceramic fibers, Int. J. Ceram. Eng. Sci. 4 (2022) 315–326.
[31] C. Sugie, A. Navrotsky, S. Lauterbach, H.-J. Kleebe, G. Mera, Structure and thermodynamics of silicon oxycarbide polymer-derived ceramics with and without mixed-bonding, Materials 14 (2021) 4075.
[32] S. Widgeon, G. Mera, Y. Gao, E. Stoyanov, S. Sen, A. Navrotsky, R. Riedel, Nanostructure and energetics of carbon-rich SiCN ceramics derived from

polysilylcarbodiimides: role of the nanodomain interfaces, Chem. Mater. 24 (2012) 1181–1191.
[33] M. Niu, H. Wang, J. Chen, L. Su, D. Wu, A. Navrotsky, Structure and energetics of SiOC and SiOC-modified carbon-bonded carbon fiber composites, J. Am. Ceram. Soc. 100 (2017) 3693–3702.
[34] H.-J. Kleebe, Y.D. Blum, SiOC ceramic with high excess free carbon, J. Eur. Ceram. Soc. 28 (2008) 1037–1042.
[35] G.A. Zank, Preceramic polymer — derived silicon oxycarbides, in: R.G. Jones, W. Ando, J. Chojnowski (Eds.), Silicon-Contain. Polym. Sci. Technol. Their Synth. Appl., Springer Netherlands, Dordrecht, 2000, pp. 697–726.
[36] D.R. Bujalski, S. Grigoras, W. (nancy) Lee, G.M. Wieber, G.A. Zank, Stoichiometry control of SiOC ceramics by siloxane polymer functionality, J. Mater. Chem. 8 (1998) 1427–1433.
[37] E. Barrios, L. Zhai, A review of the evolution of the nanostructure of SiCN and SiOC polymer derived ceramics and the impact on mechanical properties, Mol. Syst. Des. Eng. 5 (2020) 1606–1641.
[38] E.I. Ricohermoso, F. Klug, H. Schlaak, R. Riedel, E. Ionescu, Electrically conductive silicon oxycarbide thin films prepared from preceramic polymers, Int. J. Appl. Ceram. Technol. 19 (2022) 149–164.
[39] O. Eterigho-Ikelegbe, R. Trammell, S. Bada, Preparation and characterization of ceramic composites from South Africa coal discard, Construct. Build. Mater. 302 (2021), 124164.
[40] I.W. Donald, P.W. McMillan, Ceramic-matrix composites, J. Mater. Sci. 11 (1976) 949–972.
[41] L. David, R. Bhandavat, U. Barrera, G. Singh, Silicon oxycarbide glass-graphene composite paper electrode for long-cycle lithium-ion batteries, Nat. Commun. 7 (2016), 10998.
[42] R. Bhandavat, G. Singh, Stable and efficient Li-ion battery anodes prepared from polymer-derived silicon oxycarbide–carbon nanotube shell/core composites, J. Phys. Chem. C 117 (2013) 11899–11905.
[43] T. Varga, A. Navrotsky, J.L. Moats, R.M. Morcos, F. Poli, K. Müller, A. Saha, R. Raj, Thermodynamically stable SixOyCz polymer-like amorphous ceramics, J. Am. Ceram. Soc. 90 (2007) 3213–3219.
[44] R.M. Morcos, A. Navrotsky, T. Varga, Y. Blum, D. Ahn, F. Poli, K. Müller, R. Raj, Energetics of SixOyCz polymer-derived ceramics prepared under varying conditions, J. Am. Ceram. Soc. 91 (2008) 2969–2974.
[45] J.D. Torrey, R.K. Bordia, Processing of polymer-derived ceramic composite coatings on steel, J. Am. Ceram. Soc. 91 (2008) 41–45.
[46] A. Navrotsky, Progress and new directions in calorimetry: a 2014 Perspective, J. Am. Ceram. Soc. 97 (2014) 3349–3359.
[47] R. Michelle Morcos, G. Mera, A. Navrotsky, T. Varga, R. Riedel, F. Poli, K. Müller, Enthalpy of formation of carbon-rich polymer-derived amorphous SiCN ceramics, J. Am. Ceram. Soc. 91 (2008) 3349–3354.
[48] J. Chen, S.W. King, E. Muthuswamy, A. Koryttseva, D. Wu, A. Navrotsky, Thermodynamic stability of low-k amorphous SiOCH dielectric films, J. Am. Ceram. Soc. 99 (2016) 2752–2759.
[49] E. Ionescu, S. Bernard, R. Lucas, P. Kroll, S. Ushakov, A. Navrotsky, R. Riedel, Polymer-derived ultra-high temperature ceramics (UHTCs) and related materials, in: F. Baino, M. Tomalino, D. Tulyaganov (Eds.), Ceram. Glass Glass-Ceram. Early Manuf. Steps Mod. Front., Springer International Publishing, Cham, 2021, pp. 281–323.
[50] X. Guo, S. Szenknect, A. Mesbah, S. Labs, N. Clavier, C. Poinssot, S.V. Ushakov, H. Curtius, D. Bosbach, R.C. Ewing, P.C. Burns, N. Dacheux, A. Navrotsky, Thermodynamics of formation of coffinite, USiO4, Proc. Natl. Acad. Sci. USA 112 (2015) 6551–6555.
[51] A. Navrotsky, Progress and new directions in high temperature calorimetry, Phys. Chem. Miner. 2 (1977) 89–104.
[52] L.G. Benning, V.R. Phoenix, N. Yee, M.J. Tobin, Molecular characterization of cyanobacterial silicification using synchrotron infrared micro-spectroscopy1 1Associate editor, in: J.P. Amend (Ed.), Geochim. Cosmochim. Acta. vol. 68, 2004, pp. 729–741.
[53] J. Osswald, K.T. Fehr, FTIR spectroscopic study on liquid silica solutions and nanoscale particle size determination, J. Mater. Sci. 41 (2006) 1335–1339.
[54] J. Lubguban, T. Rajagopalan, N. Mehta, B. Lahlouh, S.L. Simon, S. Gangopadhyay, Low-k organosilicate films prepared by tetravinyltetramethylcyclotetrasiloxane, J. Appl. Phys. 92 (2002) 1033–1038.
[55] M. Mastalerz, R. Marc Bustin, Electron microprobe and micro-FTIR analyses applied to maceral chemistry, Int. J. Coal Geol. 24 (1993) 333–345.
[56] P.S. Thomas, J.-P. Guerbois, G.F. Russell, B.J. Briscoe, FTIR study of the thermal degradation of poly(vinyl Alcohol), J. Therm. Anal. Calorim. 64 (2001) 501–508.
[57] Y. Chen, L.d. Caro, M. Mastalerz, A. Schimmelmann, A. Blandón, Mapping the chemistry of resinite, funginite and associated vitrinite in coal with micro-FTIR, J. Microsc. 249 (2013) 69–81.
[58] E. Mendelovici, R.L. Frost, J.T. Kloprogge, Modification of chrysotile surface by organosilanes: an IR–photoacoustic spectroscopy study, J. Colloid Interface Sci. 238 (2001) 273–278.
[59] X.C. Wu, R.Q. Cai, P.X. Yan, W.M. Liu, J. Tian, SiCN thin film prepared at room temperature by r.f. reactive sputtering, Appl. Surf. Sci. 185 (2002) 262–266.
[60] C.A. Canaria, I.N. Lees, A.W. Wun, G.M. Miskelly, M.J. Sailor, Characterization of the carbon–silicon stretch in methylated porous silicon—observation of an anomalous isotope shift in the FTIR spectrum, Inorg. Chem. Commun. 5 (2002) 560–564.
[61] H. Li, L. Zhang, L. Cheng, Y. Wang, Z. Yu, M. Huang, H. Tu, H. Xia, Polymer–ceramic conversion of a highly branched liquid polycarbosilane for SiC-based ceramics, J. Mater. Sci. 43 (2008) 2806–2811.
[62] M. Mahmoudi, S. Kim, A.M. Arifuzzaman, T. Saito, C.L. Cramer, M. Minary-Jolandan, Processing and 3D printing of SiCN polymer-derived ceramics, Int. J. Appl. Ceram. Technol. 19 (2022) 939–948.
[63] P. Colombo, Polymer Derived Ceramics: from Nano-Structure to Applications, DEStech Publications, Inc, 2010.
[64] P.V.W. Sasikumar, G. Blugan, N. Casati, E. Kakkava, G. Panusa, D. Psaltis, J. Kuebler, Polymer derived silicon oxycarbide ceramic monoliths: microstructure development and associated materials properties, Ceram. Int. 44 (2018) 20961–20967.
[65] M. Li, L. Cheng, F. Ye, Y. Wang, C. Zhang, Tailoring dielectric properties of PDCs-SiCN with bimodal pore-structure by annealing combined with oxidation, J. Eur. Ceram. Soc. 40 (2020) 5247–5257.
[66] A. Saha, R. Raj, Crystallization maps for SiCO amorphous ceramics, J. Am. Ceram. Soc. 90 (2007) 578–583.
[67] R. Sreeja, T. Jayalatha, D. Devapal, Silicon oxycarbide (SiOC) foam from methylphenylpoly(silsesquioxane)(PS) by direct foaming technique, J. Porous Mater. 30 (2023) 211–221.
[68] X. Sun, G. Yang, Z. Tian, W. Zhu, D. Su, In-situ formation of titanium carbide in carbon-rich silicon oxycarbide ceramic for enhanced thermal stability, J. Eur. Ceram. Soc. 42 (2022) 6935–6941.
[69] A.Y. Lee, K. Yang, N.D. Anh, C. Park, S.M. Lee, T.G. Lee, M.S. Jeong, Raman study of D* band in graphene oxide and its correlation with reduction, Appl. Surf. Sci. 536 (2021), 147990.
[70] S. Bin Mujib, F. Ribot, C. Gervais, G. Singh, Self-supporting carbon-rich SiOC ceramic electrodes for lithium-ion batteries and aqueous supercapacitors, RSC Adv. 11 (2021) 35440–35454.
[71] Z. Sang, Z. Zhao, D. Su, P. Miao, F. Zhang, H. Ji, X. Yan, SiOC nanolayer wrapped 3D interconnected graphene sponge as a high-performance anode for lithium ion batteries, J. Mater. Chem. A. 6 (2018) 9064–9073.
[72] G. Greczynski, L. Hultman, C 1s peak of adventitious carbon aligns to the vacuum level: dire consequences for material's bonding assignment by photoelectron spectroscopy, ChemPhysChem 18 (2017) 1507–1512.
[73] D.J. Morgan, Comments on the XPS Analysis of Carbon Materials, C, vol. 7, 2021, p. 51.
[74] H. Zhao, L. Chen, X. Luan, X. Zhang, J. Yun, T. Xu, Synthesis, pyrolysis of a novel liquid SiBCN ceramic precursor and its application in ceramic matrix composites, J. Eur. Ceram. Soc. 37 (2017) 1321–1329.
[75] H. Wang, W. Zhu, X. Sun, D. Su, Preparation of aerogel-like SiOC ceramic with honeycomb structure and its high-temperature performance, J. Alloys Compd. 937 (2023), 168438.
[76] X. Zhang, D. Wang, X. Qiu, Y. Ma, D. Kong, K. Müllen, X. Li, L. Zhi, Stable high-capacity and high-rate silicon-based lithium battery anodes upon two-dimensional covalent encapsulation, Nat. Commun. 11 (2020) 3826.
[77] M. Kollep, G. Konstantinou, J. Madrid-Wolff, A. Boniface, L. Hagelüken, P.V. W. Sasikumar, G. Blugan, P. Delrot, D. Loterie, J. Brugger, C. Moser, Tomographic volumetric additive manufacturing of silicon oxycarbide ceramics, Adv. Eng. Mater. 24 (2022), 2101345.
[78] T.S. Key, G.B. Wilks, M.K. Cinibulk, Effect of pendant groups on the mass yield and density of polycarbosilanes during pyrolysis, J. Am. Ceram. Soc. 105 (2022) 2403–2410.